



NUMERICAL SIMULATION OF CENTRIFUGAL COMPRESSOR

Srinivas G.

Department of Aeronautical Engineering, MIT-Manipal University, Manipal, Udupi, Karnataka, India

E-Mail: srinivasle06@gmail.com

ABSTRACT

Design of 3D-centrifugal impeller blades is a compromise between manufacturability and aerodynamics. The aerodynamic requirement is that edge velocities along the impeller channel passage surfaces like hub, shroud, pressure and suction surfaces vary smoothly without sudden decelerations, which would otherwise cause flow separation leading to losses. The paper aims to study several flow characteristics between blade channels using commercial flow solver CFX based on finite volume techniques. From the public domain literature, using the blade data, profiles are developed, for which multiblock hexahedral computational meshes are generated. Using the periodic boundaries and defined flow conditions at inflow / exit flow and blade rotations, the turbulent viscous flow between blade channels are computed. The efficiency related parameters using average quantities, besides flow pattern in terms of velocities, streamlines and pressure distribution on blade surfaces are graphically interpreted. An attempt is also made to study the influence of pressure loads on structural deformations in the chosen blade profile. This analysis also provides insights into the locations of maximum principal stresses or equivalent stresses on blade surfaces. This paper highlights aero-mechanical features of centrifugal impeller obtained from several numerical simulations, which are expected to provide a sound basis for further investigations.

Keywords: centrifugal compressor, CFX, multiblock, blades, streamlines.

INTRODUCTION

The gas turbine engines powering the most passenger and military aircrafts are also called jet engines. All jet engines have a compressor to increase the pressure of the incoming air. There are two compressor designs found in jet engines as shown in Figure-1, which are axial type wherein airflow is parallel and centrifugal type wherein airflow is perpendicular to the axis of rotation. In centrifugal compressor due to the low efficiency and thrust-to weight ratio, they are limited to short range applications [1]. However, the inability for spark ignition engines to work at high altitude warrants further development to improve the efficiency of these miniature gas turbines. Furthermore, gas turbines in the form of turbojet or turbofan are capable of providing propulsion at higher speed, where spark ignition engines are not applicable with air screws.

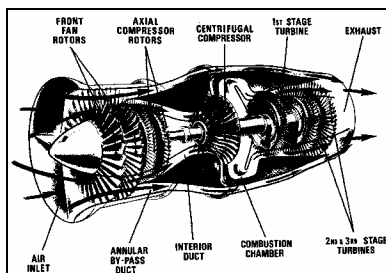


Figure-1. Jet engine centrifugal compressor

MODELING OF COMPRESSOR BLADES

Based on public domain literature on design of compressor blades used in aero engines, typical blade profile is constructed using the template based software module built in ANSYS workbench-12 version [2]. The blade gen layout with construction features related to

wrapper angle, number of blades, angles distribution and blade thickness for generation of three dimensional blades was done as shown Figure-3 in order to carry out structural analysis of the blade surfaces the software provided export options to generate computational mesh accounting blade thickness is also explored in static structural analysis package.

The blade profiles generated in above software module are imported to template based multi-block structured computational mesh software module called turbo grid. The information related to machine data, profile curves, several inputs required for width factor periodicity production, topology freezing for generation of geometric representation in terms of surface mesh generation with master and slave control points being generated. default orientation of master and slave control points on the blade surfaces are to be moved to obtain better orthogonally between mesh points. After these operations three dimensional computational mesh generation process for compressor blade with boundary patches, periodic surfaces are created.

MESHING OF COMPRESSOR BLADES

The three dimensional mesh generated for compressor blade is imported into the ANSYS Pre-processor using Turbo setup. In this process the grid data is read and checked for right handed coordinate system and scaling the grid data into SI units, domain setup with material properties required are highlighted. The surface mesh of blade inlet, exit, blade, left and right periodic and hub and shroud surfaces are visualized as shown in Figure-2. The compressor impeller with multiple blades in shaded view is shown in Figure-3.

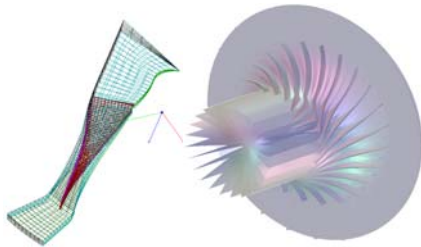


Figure-2, 3. Surface grid single Blade, Shaded view of 3d compressor blades.

The blade geometry designed has been saved as .bgd file for future modifications and shape optimization. For further analysis, the .bgd file can be exported as hub, shroud, profile and periodic curves to Turbogrid module where space discretization can be carried out which in turn can be exported to CFD flow simulation. In addition to this, this software also exports as IGES file for discretization of computational mesh with structured multi block mesh for blade thickness for structural analysis. Thus for rapid analysis, this software module provides detailed 3D solid modeling geometry components for maximum accuracy when assessing a particular design.

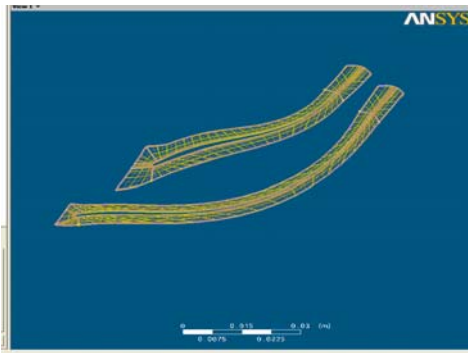


Figure-4. Compressor blade surface with improved control points.

The control points on the periodic line should be positioned, e.g. in the middle of the blade passage. Selecting the options-show-duplicate blade option will give guidance to locate the mid passage points. The O-grid at leading and trailing edge control points should be positioned at the approximate 45 degree position around the leading and trailing edge radius. The O-grid mid-channel control points should be positioned to make mid-channel control curve perpendicular to the O-grid. The near blade upstream and downstream control curves should bisect the angle between the O-grid and the channel boundary. After the modifications to control points to improve minimum face angles and selecting the mesh size options the resulting topology for blade hub and shroud surfaces are shown in Figure-4 wherein it is observed that percentage of bad elements is zero

Volume mesh has been generated and shown for the single blade row in the Figure-5. The mesh quality in terms of skew angles, aspect ratio and right-handed ness

was checked and the grid data was found to be within tolerances. The mesh has been exported as .gtm file for further pre-processing in the Ansys CFD pre and solver software package.

COMPUTATIONAL MESH FOR STRUCTURAL ANALYSIS

Most fluid flow simulation technology uses completely different meshing, loading and solving methods compared to structural simulation. And this is where the true power of Workbench 12.0 comes into play. When the user is connecting up the dialogs within the schematic layouts, many of these are handled automatically, simply by dragging a connection between the outputs of one analysis system and the inputs of another. When and if there's mapping to be done, this is handled in a very simple dialog that makes the process simple, rather than the often-tortuous methods traditionally associated with this type of work [2]. There are no geometry creation tools in the Mechanical application and so geometry must be attached to the Mechanical application. The geometry from either of the CAD Systems and Blade Gen Model can be connected to simulation model before setup option is activated.

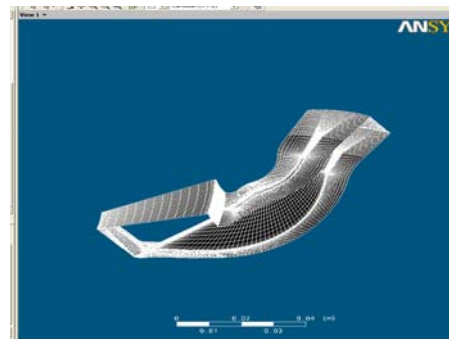


Figure-5. Three dimensional mesh for single compressible blade row.

The next step is to generate the meshing solid body for which several methods are provided in ANSYS Workbench these tools have the benefit of being highly automated along with having a moderate to high degree of user control. Upon startup of the meshing application meshing options panel displays, which allows you to quickly and easily set your meshing preferences based on the physics you are preparing to solve. For solid bodies, the software uses meshing techniques based on algorithms and element shape. One of the technique extensively used are called patch independent meshing for the part using tetrahedral element.

The default value selects meshing control parameters and provides a successful automated mesh. By default, the application attempts to use auto sweeping for solid models and quadrilateral element generation for surface body models. If a model is not sweepable, the Patch Conforming mesher under Tetrahedrons is used.



Then one needs to change the default values suitably in the Mesh option panel.

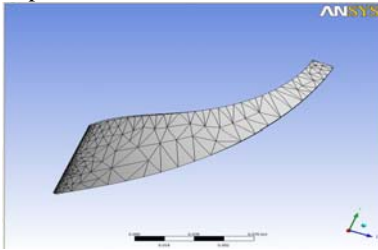


Figure-6. Three dimensional mesh on the blade with thickness.

Patch independent mesh are defined by max element size and number of elements. The default value is calculated from the diagonal length of the bounding box which is based on the initial seed settings of mesh object folder. When curvature and proximity refinement options enabled, the mesh automatically refined based on geometry. This will result in larger elements on flat planar faces and smaller elements in areas of high curvature or within small gaps. However projection to geometry and smoothing may push the size even smaller for some of the elements as observed in blade leading edges.

OVERVIEW OF FLUID MECHANICS FOR TUBOMACHINERY

All The transport of fluid comprises gases/liquid from one component to other in power/process equipment are described through mass, momentum and energy conservation principles. The Navier Stokes (transport) equations are derived from these principles and are discussed by Hoffman, K.A (1993) which are represented mathematically as:

$$\frac{\partial \rho \phi}{\partial t} + \text{div}(\rho \phi \vec{u}) = \text{div}(\Gamma \text{grad} \phi) + q_{\phi} \quad (1)$$

The terms on Left Hand Side (LHS) defines acceleration of flow over time with inertia depends on the sum of the external forces, diffusion and sources acting on the fluid element. If the value of ϕ is 1, the equation (1) results in continuity equation. If the value of ϕ is either u or v or w, the above equation describes momentum equation in x, y, z directions. If the value of ϕ is h then the above eqn. yields to energy equation. Two important material properties of fluid i.e., density and viscosity, whose ratio times characteristic flow velocity and length are defined as Reynolds number. This non-dimensional quantity is the ratio of inertial forces to viscous forces, whose magnitude depends upon flow disturbances, can change the flow from laminar to turbulent. In other words, if the Reynolds Number is small, then the flow will be laminar, meaning that the flow progresses in layers [6].

If the Reynolds Number is large then the flow will be turbulent, meaning there will be a mixing of flow layers and the creation of large eddies. The flow consists

of a spectrum of different scales in turbulent flow, largest eddies are the order of geometry scales and breaks into smaller as time progress. At the other end of the spectra, the smallest eddies by viscous forces dissipated into internal energy. Even though turbulence is chaotic, its characteristics are determined through Navier-Stokes equations. The turbulence is dissipative, which means that kinetic energy in the small eddies are transformed into internal energy. The small eddies receive the kinetic energy from slightly larger eddies. The slightly larger eddies receive their energy from even larger eddies and so on. In order to resolve wide spectrum of scales in turbulent eddies, normally two approaches are employed

This requires dense mesh points for proper resolution and its solution depends on heavy computational resources that are expensive, time consuming process and therefore very rarely used simulation technique. The other approach generally used for most of the applications are Reynolds' averaging process wherein flow variables are decomposed into mean and fluctuating components as:

$$u_i = \bar{u}_i + u_i' \quad (2)$$

Where i=1,2, 3 denotes in x, y, z direction [7]. Likewise the pressure and other scalars can be expressed as:

$$\phi = \bar{\phi} + \phi' \quad (3)$$

Substituting flow variables in this form into the instantaneous continuity and momentum equations and taking a time (or ensemble) average (and dropping the over bar on the mean velocity) yields to:

$$\frac{\partial \rho}{\partial t} + \frac{\partial}{\partial x_i} (\rho u_i) = 0 \quad (4)$$

$$\frac{\partial}{\partial t} (\rho u_i) + \frac{\partial}{\partial x_j} (\rho u_i u_j) = -\frac{\partial p}{\partial x_i} - \frac{\partial}{\partial x_j} \left[\mu \left(\frac{\partial u_i}{\partial x_j} + \frac{\partial u_j}{\partial x_i} - \frac{2}{3} \delta_{i,j} \frac{\partial u_l}{\partial x_l} \right) \right] + \frac{\partial}{\partial x_j} (\overline{\rho u_i' u_j'}) \quad (5)$$

Equation (4), (5) are called RANS equations. The term $\overline{\rho u_i' u_j'}$ in the equation (5) results from averaging process and is called Reynolds' Stress. With the help of Boussinesq hypothesis to relate the Reynolds stresses, choosing Kronecker delta $\delta=1$ if $i=j$ and $\overline{u_i' u_i'} = 2k$ the Reynold's stress term in the equation (5) is rewritten as:

$$-\overline{\rho u_i' u_j'} = \mu_t \left(\frac{\partial u_i}{\partial x_j} + \frac{\partial u_j}{\partial x_i} \right) - \frac{2}{3} \left(\rho k + \mu_t \frac{\partial u_k}{\partial x_k} \right) \delta_{i,j} \quad (6)$$



where μ_t is turbulent viscosity. To resolve turbulence viscosity and Reynolds' stresses, eddy viscosity models based on Boussinesq hypothesis will lead to zero, one and two equation turbulence models and Reynolds's Stress Models (RSM). The strength and weakness of these models for prediction of turbulence effects are extensively studied.

Whenever non-isotropic effects are important use of higher models like $v^2 - f$ is preferable to predict separation near the wall. When the fluid flow is subjected to rotating components, Large Eddy Simulation (LES) or Detached Eddy Simulations (DES) is employed to evaluate flow characteristics as a function of turbulence viscosity and energy dissipation. These models are based on filtered equations, which still require finer meshes to solve RANS calculations in transient mode. In the simulation of turbulent flows, accurate estimation of pressure drop is highly dependent on usage of turbulence model with smooth/rough wall functions.

STRUCTURAL DEFORMATIONS DUE TO FLOW PRESSURE LOADS - FSI

The mathematical formulations to simulate structural deformations and stresses on the component surfaces are extensively discussed in the literature. To determine the deformations, the governing equations are mathematically represented as:

$$\rho \ddot{u} = \nabla \cdot \sigma + b \quad (10)$$

where \ddot{u} is displacement, σ is stress field that depends on strain, internal variable, b - body force. The expression for strain in terms of displacement can be expressed as:

$$\bar{\varepsilon} = \frac{1}{2} (\nabla \ddot{u} + \nabla \ddot{u}^T) \quad (11)$$

The finite volume form and after integration by parts, the equation (19) can be written as:

$$\int_V \rho \ddot{u} dV = \int_A \sigma ds + \int_V b dV \quad (12)$$

For all cells i in the domain V , the discrete form of the momentum equation become:

$$\rho_i \ddot{u}_i V_i = \sum_{j \in f(i)} f_j + b_i V_i \quad \text{where } f_j = \sigma_j \cdot s_j; \quad (13)$$

s - surface vector

Dropping inertial terms and considering some of the forces acting on the body are zero for a static case, the equation (13) can be re-written as:

$$r_j = \sum_{j \in f(i)} f_j + b_i V_i \quad (13)$$

In order to compute the stress tensor $\bar{\varepsilon}$ on the centroids of the faces, it is required to establish the discrete form of the strain tensor and the deformation gradient $\nabla \ddot{u}$. The deformation gradient is computed at cell centers based on the difference in displacement between neighboring points. The approximation of stiffness matrix can be accumulated over all faces are:

$$K_{ik} = - \frac{\partial r_i}{\partial u_k} = - \sum_{j \in f(i)} \frac{\partial f_j}{\partial u_k} \quad \forall_{i,k} \in N(i) \quad (14)$$

With the help of Newton method to correct displacement equation (14) further simplifies to:

$$K_{i,k} \nabla \ddot{u}_k = r_i^n; \quad \nabla \ddot{u}_k = \ddot{u}_k^{n+1} - \ddot{u}_k^n \quad (15)$$

To obtain structural deformations, pressure/heat flux loads are normally obtained from CFD solver using finite volume approximations and deformations/stresses are obtained through finite element techniques. However, in the current versions of few flow solvers, flow and thermal stress based on finite volume techniques can provide FSI characteristics of industrial components.

FLOW SIMULATION IN CENTRIFUGAL COMPRESSOR BLADE

The three dimensional mesh generated for compressor blade is imported into the ANSYS Pre-processor using Turbo setup. In this process the grid data is read and checked for right handed coordinate system and scaling the grid data into SI units. Among several boundary conditions applied for flow simulation blade wall rotation about Z-axis with specified revolution per minute is accounted.

The boundary conditions determine to a large extent the characteristics of the solution you obtain. Therefore, it is important to set boundary conditions that accurately reflect the real situation to allow you to obtain accurate results.

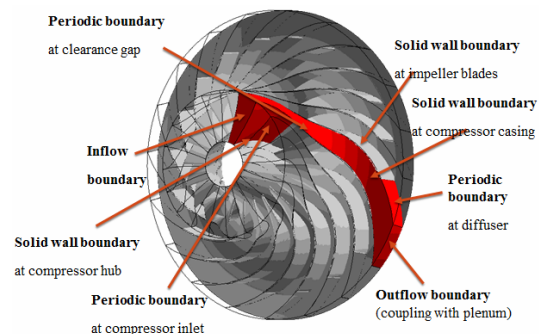


Figure-7. Boundary conditions (Flow Solver).

Boundary conditions must be applied to all the bounding regions of the computational domain. Boundary conditions can be inlets, outlets, openings, walls and



symmetry planes as shown in Figure-7. For a given computational domain, boundary conditions can be given that over-specify or under-specify the problem. This usually results in non-physical solutions or failure of the solution to converge.

To predict viscous losses industry standard two equation turbulence model has been employed. With suitable initial guess and under relaxation parameters, flow and energy equations are iterated till the residual errors are dropped to the order of $1e-04$ shown in figure from 8-10.

After completion of flow simulation a macro built in the software for generations of report is activated to obtain performance and efficiency calculations. The variations in the rotational speed of the blade has been accounted to predict total pressure ratio and Isentropic efficiency of the blade is estimated and plots generated to understand the phenomena of choking and surging.

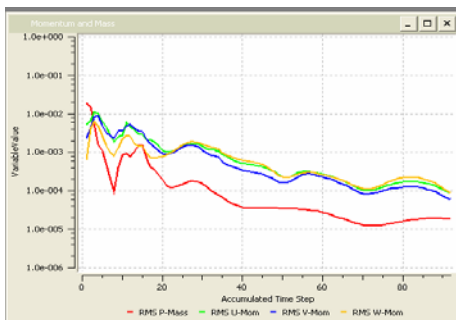


Figure-8. Momentum and mass converged residual plot.

The influence of pressure loading on the blades for structural integrity is examined using linear static structural analysis module built in ANSYS workbench. The process of taking blade geometry in structural simulation is connected first and later CFX result file was imported. Setup is activated so as to obtain the geometry of the blade along with fluid-solid surfaces in structural simulation module.

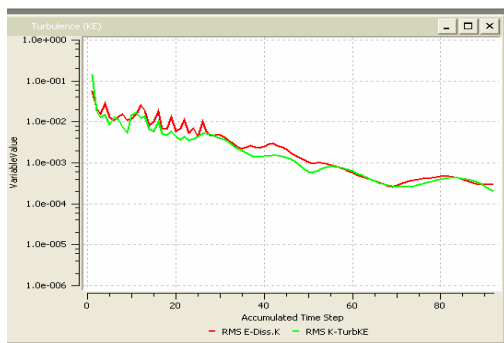


Figure-9. Turbulence converged residual plot.



Figure-10. Heat transfer converged residual plot.

Automatic methods to generate computational mesh for blade along with thickness are used and applied to get imported pressure load on blade surface. Blade is constrained through fixed support and using inertial option wall rotations are defined. With this physics setup and material properties simulations has been carried out for Total displacement and equivalent stresses. The results obtained for blade deformations and maximum and minimum stress levels are interpreted graphically.

RESULTS AND DISCUSSIONS

The impellor blades are rotating with 22000 rpm is subjected to mass flow 0.167 kg/s with the working pressure is of order 1 atm. The pressure loading over stream wise directions for the span of 20%, 50% and 80% are shown in the Figures 11-13. The pressure profiles on the surfaces near hub mean and tip region provides details of boundary layer separation with steep adverse pressure gradients [5].

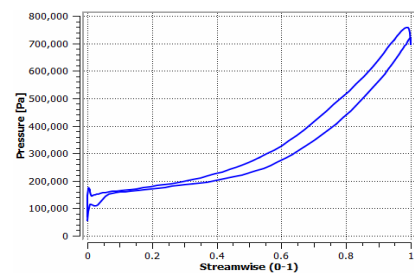


Figure-11. Pressure loading over stream wise loading span of 20%.

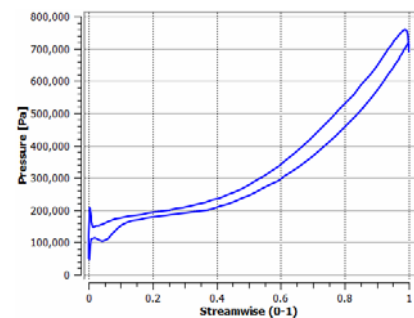


Figure-12. Pressure loading stream wise loading span of 50%.

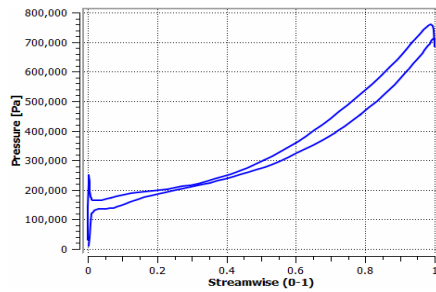


Figure-13. Pressure loading over streamwise loading span of 100%.

Both Figures 15-16 show the pressure and efficiency curve features of typical centrifugal compressors, where pressure and efficiency peak at a certain flow rate. Increasing or decreasing the flow rate from this optimum point results in a reduction in both pressure and efficiency.

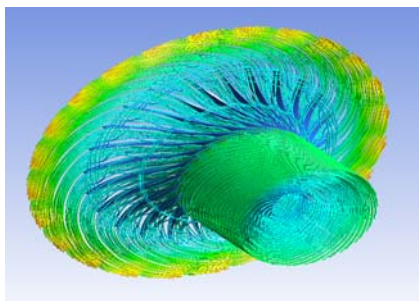


Figure-14. 3D streamlines from the inlet of impeller around the blades.

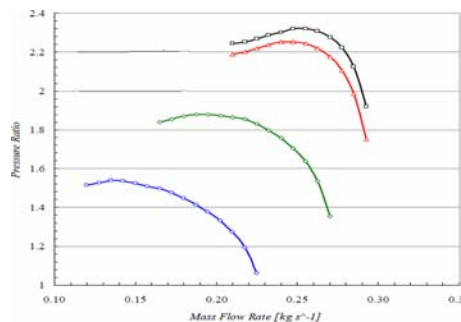


Figure-15. Pressure ratio mass flow curve of the compressor.

Pressure drops rapidly with the increase in mass flow rate and this will lead to choking at a certain point. On the other hand, pressure also drops accordingly as the mass flow rate is reduced from that optimum point and the stage will quickly start to surge. The exact points for surging and choking would not be predicted.

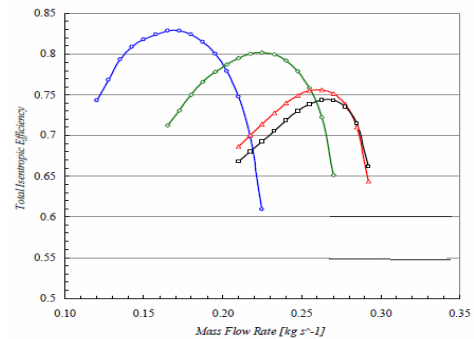


Figure-16. Stage efficiency curves.

CONCLUSIONS

The application of centrifugal compressor with backward sweep twisted blade in turbofan and its performance of air motion from upstream components are described based on published literature. Simulation for different rotational speeds with the variations in mass flow, the pressure and efficiency curve features of typical centrifugal compressors, show that the pressure and efficiency have peak at a certain flow rate.

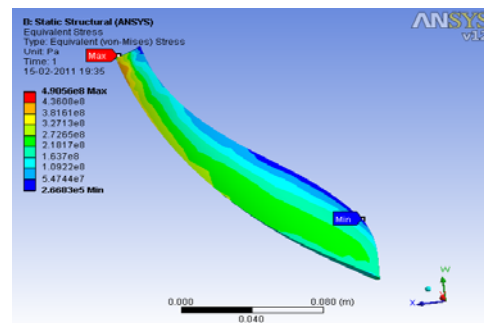


Figure-17. Equivalent stress under blade surface.

Increasing or decreasing the flow rate from this optimum point results in a reduction in both pressure and efficiency. Pressure drops rapidly with the increase in mass flow rate and this leads to choking at a certain point. On the other hand, pressure also drops accordingly as the mass flow rate is reduced from that optimal point and the stage quickly starts to surge.

It is observed that maximum stress is taking place at the hub surface trailing edge and minimum stress is noticed on shroud surface when pressure load obtained from CFD solution is specified on the blade surfaces is shown in Figure-17. As mass flow varies at constant rotational speeds the magnitude of maxima and minima of stresses decrease. Similarly, the total deformation also decreases at constant speed at different mass flow rates.

REFERENCES

- [1] D. Japikse. 1996. Centrifugal Compressor Design and Performance. Concepts ETI Inc.



- [2] R. Aungier. 2000. Centrifugal Compressors: A Strategy for Aerodynamic Design and Analysis. ASME.
- [3] D. Flaxington and E. Swain. 1999. Turbocharger Aerodynamic Design. Proc. Instn Mech Engrs. 213(Part C): pp. 43-57.
- [4] P. Dalbert, B. Ribí, T. Kmeci and M.V. Casey. 1999. Radial Compressor Design for Industrial Compressor. Proc Instn Mech Engrs. 213(Part C): 71-83.
- [5] P.M. Came and C.J. Robinson. 1999. Centrifugal Compressor Design. Proc. Instn of Mech. Engrs. 213(Part C): 139-155.
- [6] A. Lohmberg, M. Casey and S. Ammann. 2003. Transonic Radial Compressor Inlet Design. Proc Instn of Mech Engrs. 217(Part A): 367-374.
- [7] J.D Denton and W.N. Dawes. 1999. Computational Fluid Dynamics for Turbomachinery Design. ProcInstn of Mech. Engrs. 213(Part C): 107-124.